Manufacturing Rev. **11**, 19 (2024)

https://doi.org/10.1051/mfreview/2024018

Manufacturing Review
Available online at:
https://mfr.edp-open.org

RESEARCH ARTICLE OPEN ACCESS

Mechanical characteristics of dissimilar friction stir welding processes of aluminium alloy [AA 2024-T351 and AA 7075-T651]

Getachew Gebreamlak, Sivaprakasam Palani*, and Belete Sirahbizu

Department of Mechanical Engineering, College of Engineering, Nanotechnology Centre of Excellence, Addis Ababa Science and Technology University, P.O. Box 16417, Addis Ababa, Ethiopia

Received: 27 November 2023 / Accepted: 23 July 2024

Abstract. Aerospace industries have remained dependent on aluminium alloys for airframe structural components manufacturing due to their superior strength, fracture toughness, and ability to resist corrosion. Especially, AA2024 and AA7075 have been the most prominent and timely tested robust aluminium alloys in these manufacturing sectors. However, joining these aluminium alloys through conventional fusion welding is difficult. The present investigation focused on the mechanical and metallurgical properties of these high-strength dissimilar aluminium alloys 2024-T351 and 7075-T651 using a Friction Stir Welding (FSW) process. The effects of factors such as rotational speed RS (800–1200 rpm), welding speed WS (20–60 mm/min), and tool plunge depth (0.2–0.4 mm) on the ultimate tensile strength (UTS) and yield strength (YS) have been evaluated. The experimental procedure employed is based on RSM. The fractured surface morphology was investigated using SEM. The investigation result showed higher tensile strength (147 MPa) at the combination of welding parameters (1200 rpm, 60 mm/min, and 0.4 mm). The fabrication industries became the great beneficiaries of this emerging technology of the FSW.

Keywords: Surface morphology / ultimate tensile strength / aluminium alloy / ANOVA / friction stir welding

1 Introduction

Friction stir welding (FSW) is a solid-state joining system for various materials, including metals and metal alloys. For structurally demanding applications, it is currently expanded to include a variety of similar and dissimilar material combinations [1,2]. A defining characteristic of FSW is that the cylindrical rotating tool creates the welded joint and mechanically traverses into the materials. As a result of the frictional surface between workpiece materials and the FSW tool [shoulder-pin], heat is produced [3,4]. A solid cylindrical tool with a shoulder and a profiled pin (smaller diameter) projecting from the tool shoulder is used in the method, which is depicted in Figure 1. This creative and innovative joining method lowers the material's melting point and eliminates welding defects in typical fusion welding approaches.

Aluminum series 2xxx and 7xxx are a significant class of alloys widely used in the aerospace industries where advanced weight reduction techniques for airframe structural component manufacturing are crucial. The AA7xxx series alloys are typically selected due to their exceptional strength. In contrast, the AA2xxx series alloys are typically assigned to applications where fatigue poses a significant challenge and elevated service temperatures may be experienced. It emerged that joining the Al alloy using typical fusion welding techniques was susceptible to defects. Hence, it demands the search for an alternative and efficient means of joining these aviation-grade aluminum alloys using FSW, where the influence of factors on FSW and the mechanical and metallurgical analysis of the welded joint are vital areas of applied research [5]. Additionally, despite the numerous independent uses of AA7075 and AA2024, the two alloys are utilized where joining these high-strength aviation aluminum alloys became vital in various demanding applications [6].

FSW has brought a new revolution for solidification-related issues, such as low joint efficiency and other flaws. According to Heidarzadeha (2021) [7], the joint efficiency made by the friction stir welding process reached as high as 100% in some metals. The other outstanding feature brought by FSW is the joining of dissimilar metals. Hence, FSW is becoming the primary choice in the application areas where the joining of dissimilar materials, particularly those with significantly diverse mechanical, physical, and chemical properties, and those in which brittle intermetallic phases occur in the weld zone are required. Moreover, further

* e-mail: shiva@aastu.edu.et

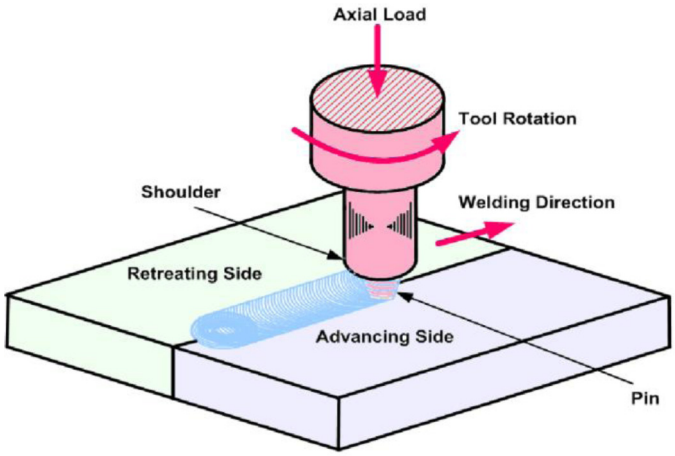

Fig. 1. FSW process schematic diagram.

research is taking place to exploit the immense benefit of FSW for other high-temperature materials, such as alloys made of titanium and steel [8,9]. Since no hazardous or poisonous chemicals or radiation are produced in friction stir welding, it has been recognized as a sustainable and ecologically friendly welding technique. Conversely, traditional arc welding methods produce dangerous radiation and fumes, including MIG, LBW, Tungsten Inert Gas (TIG), and GMAW, which can be extremely dangerous for the environment and welders [10]. The advantage of friction stir welding over traditional arc welding is that it uses less energy, produces less material waste, and has the high stability of hardening particles [11]. Commonly, porosity, fusion failure, and cracks are caused by using filler material in traditional arc welding. Nevertheless, if the proper method is followed, friction stir welding can create nearly flawless welds without flaws because it does not require filler material [12]. Friction stir welding are lessens radiation and harmful emissions, minimizes surface cleaning, and does away with grinding waste, according to Wahid et al. [13]. These are just a few of the significant environmental advantages that FSW offers. Also, FSW saves fuel in lightweight applications and permits welding on thicker material layers, contributing to energy savings. For enterprises seeking to increase production and efficiency while lessening their environmental impact, FSW is a desirable alternative because of these advantages.

With improved joint characteristics, less preparation time, no filler material usage, no fume liberation to the environment, and its capacity to join similar and dissimilar aluminum components, FSW welding is becoming an emerging technology, mainly in the automotive and aerospace sectors. Uday et al. (2022) [14] have also concentrated on the parameters used in the welding process to attain high-quality weld joints. The combination of the ideal welding speed, rotation speed, and axial load was found to vary the joint efficiency between 80% and 95%. In order to ensure uniform grain size, the study's input parameters included welding speeds of 30–110 mm/min, tool rotation speeds between 600 and 1200 rpm, and a moderate axial load. The benefits of FSW also include other welded joint's mechanical attributes. According to Anand et al. (2019) [15], the yield stress and fracture toughness of the FSW of aluminum alloy joints reached 80 to 100% of the base metal, respectively. However, it disclosed much better mechanical properties in fracture toughness and fatigue strength and became an economical choice as there is no edge preparation requirement. The other point is that FSW utilizes a few parameters compared to conventional fusion welding. However, the combination of optimum process parameters is highly regarded for the welded joint's required mechanical and micro-structural properties.

Mahany et al. [16] studied the influence of the input factors as axial load and tool RS while FSW of Al alloys 7075-T6 and 2024-T3 on the tensile strength, microhardness, and microstructure. The increasing axial load (1300 kg) and rotation speed (1200 rpm) increased the tensile strength values to 378.7 MPa. However, it abruptly decreased with increasing RS (1600 rpm) and axial load (1450 kg) because of the kissing bond defect in the SZ-TMAZ interface, excessive heat input, and tunnel defects in SZ. Though FSW became a significant concern in every fabrication industry, the greatest beneficiaries are high-strength aviation-graded aluminum alloys AA2024 and AA7075 that the conventional fusion welding failed to weld. The review [17] covered the foundational ideas, parameters, and effects of the FSW settings on the mechanical properties and microstructure. The effects of RS (600–1650 rpm) on mechanical, material-flow, and microstructure properties of tempered grades of Al alloys (AA7075-T651 and AA2024-T351) using FSW were investigated [18]. TMAZ width is greater on the retreating sides than on the advancing sides. Thus, the joint quality is greatly influenced by the rotational speed. Less material mixing occurs at low rotational speeds, and the distinctive onion ring mixing configuration is produced at high rotational speeds.

At an RS of 600 rpm, all the joints experience significant grain refinement, approximately 1.7 μm compared to the base materials. Grain coarsening is frequently the effect of increasing RS. The simple shear texture, which varies with RS, dominates any joint's crystallographic surface in the NZ. The site of tensile fractures coincides with the minimal hardness in the joints, whose hardness increases and subsequently decreases from upper to lowermost along the center direction. In the study of similar tempered grades of aluminum alloys, the evolution of the dissimilar FSW was shown to have a significant impact on tool design. Pin flute radius was studied by Hasan et al. [19] when FSW dissimilar aluminum alloys. Five pin tools were investigated through a flute radius of 0–8 mm, keeping base materials on the AS and RS sides with 900 rpm RS and 150 mm/min of WS. Microstructure and tensile property analyses were performed. It was discovered that the radius of the flutes significantly impacted weld quality. However, when the materials were positioned relative to one another, the highest-strength joint was achieved by the welding pin tool with the same radius flute [20].

Friction stir welding is an innovative and novel method for enhancing the weld joint properties of dissimilar materials compared to conventional welding. Hence, this research article focused on an experimental investigation

Table 1. The alloying element of Al alloy.

Grade	Percentage of alloying element compositions (%)									
	Al	Cr	Cu	Fe	Mg	Mn	Si	Ti	Zn	Others
AA2024-T351	90.7–94.7	0.1	3.8–4.9	0.5	1.2	1.8	0.5	0.15	0.25	0.15
AA7075-T651	87.1–91.4	0.18–0.28	1.2–2	0.5	2.1–2.9	0.5	0.4	0.2	5.1–6.1	0.15

and optimization of friction stir welding process parameters of dissimilar aluminium alloys, AA2024-T351 and AA7075-T651. The experimental procedure was performed based on an RSM-based design. Mechanical performance, such as tensile and yield tests, have been performed. The effects of FSW factors on the tensile strength (TS) and yield strength (YS) of FSWed joints were investigated. The microhardness and surface topography of weld properties have been investigated. A mathematical model was developed to predict responses, and ANOVA was used to determine the significance of the factors. The desirability approach was used to optimize and find the optimal FSW conditions of aluminium alloy.

2 Experimental procedure

2.1 FSW materials

The material used for experiments is a commercial tempered grade of aluminium alloy square plates 100×100 mm with a thickness of 6.0 mm. Table 1 indicates the compositions of each alloying element found in each aluminium alloy grade. High-strength aluminium alloys, such as the 2xxx and 7xxx family, are widely used for structural purposes, including aeroplane constructions [21,22]. These alloys are particularly useful for their dissimilar welding. Regarding joining high-strength aluminium alloys from the 2xxx and 7xx series, FSW is a potential solid-state welding technique that offers several benefits over conventional fusion welding. Both alloys (2xxx and 7xxx series) are high-intensity and heat-treatable/age-hardenable aluminium alloys and are mainly employed in the aerospace and automotive sectors and armed vehicles [23,24]. AA2xxx series is mostly used in internal components, including frames, wing stringers, and lower wing skins. These materials are frequently utilized in applications requiring excellent fracture toughness and low light weight. The AA7xxxx series was used to create aerospace parts requiring high strength, such as upper wing skins, vertical and horizontal stabilizers, and wing stringers [25]. Hence, AA 2024-T351 and AA 7075-T651 aluminium alloys were chosen for the current study.

2.2 FSW tool

The weld microstructure, characteristics, and weld quality depend on the FSW tools, typically referred to as the heart of the FSW technique [20]. The FSW tool is prepared with tool steel (AISI H13), 56 HRC, hardened and tempered, as shown in Figure 2. H13 tool steel became an ideal tool material for FSW of Al alloys, where the resulting tensile strength is the principal response variable [26]. Tool steel, H13, is chromium-based tool steel commonly used in hot work applications [27]. After being manufactured on a lathe machine, the tool was made to pass through the double tempering heat treatment process to acquire combined properties of two contradictory requirements for optimum performance: high hardness and high toughness. Table 2 presents the major alloying elements of the FSW tool.

2.3 FSW process setup

The FSW test is performed in Fanuc oi-MC Control DMTG VDF- 1200 CNC Vertical Machining Center, at Addis machine tool industry, EEG shown in Figure 3a.

2.4 Design of Experiments (DoE)

Response surface methodology (RSM) is a practical mathematical approach for modeling and analyzing issues when many factors determine a response's significance and where the objective is to improve responses [28]. The second-order RSM regression model establishes an association between the factors and the responses. The form of the RSM regression model is shown in equation (1).

$$y = \beta_0 + \sum_{i=1}^{k} \beta_i x_i + \sum_{i=1}^{k} \beta_{ii} x_i^2 + \sum_i \sum_j \beta_{ij} x_{ij} \quad (1)$$

where y for the response function, β_0 to β_{ij} stands for unknown coefficients, x_i are independent variables, k is for the number of independent variables. This study investigated the effects of process variables RS, WS and PD, on the UTS and YS of FS welded joints. The experiments were designed using a central composite design (CCD). Factors with lower and upper bounds are denoted by −1 and +1, respectively. Table 3 shows the factors and levels for FSW of dissimilar aluminum alloys using RSM. Table 4 presents the twenty experimental observations at three different input variables used and the experimental results of FSW.

2.5 Testing and characterization

The ultimate tensile strength, yield strength, and microhardness tests are used for mechanical properties analysis, and optical and SEM are used for surface topography analysis.

2.5.1 Tensile testing

The specimens have been prepared according to the ASTM E8/E8M sub-size standard (Fig. 4a) for the tensile test of FSWed joints. The universal testing machine (UTM), shown in Figure 4c, is used to test the FSWed joint's strength.

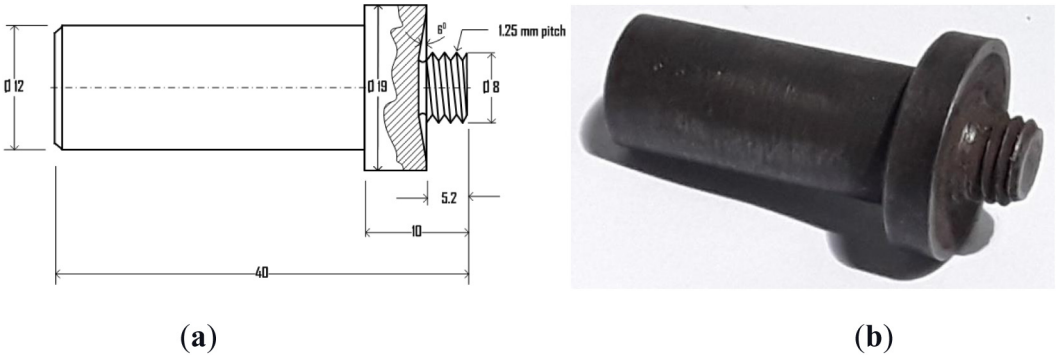

Fig. 2. (a) H13 FSW tool schematic diagram; (b) FSW tool photograph.

Table 2. Major alloying elements of tool steel (H13).

Carbon	Chromium	Molybdenum	Vanadium	Silicon
0.39%	5.4%	1.35%	1.0%	1.0%

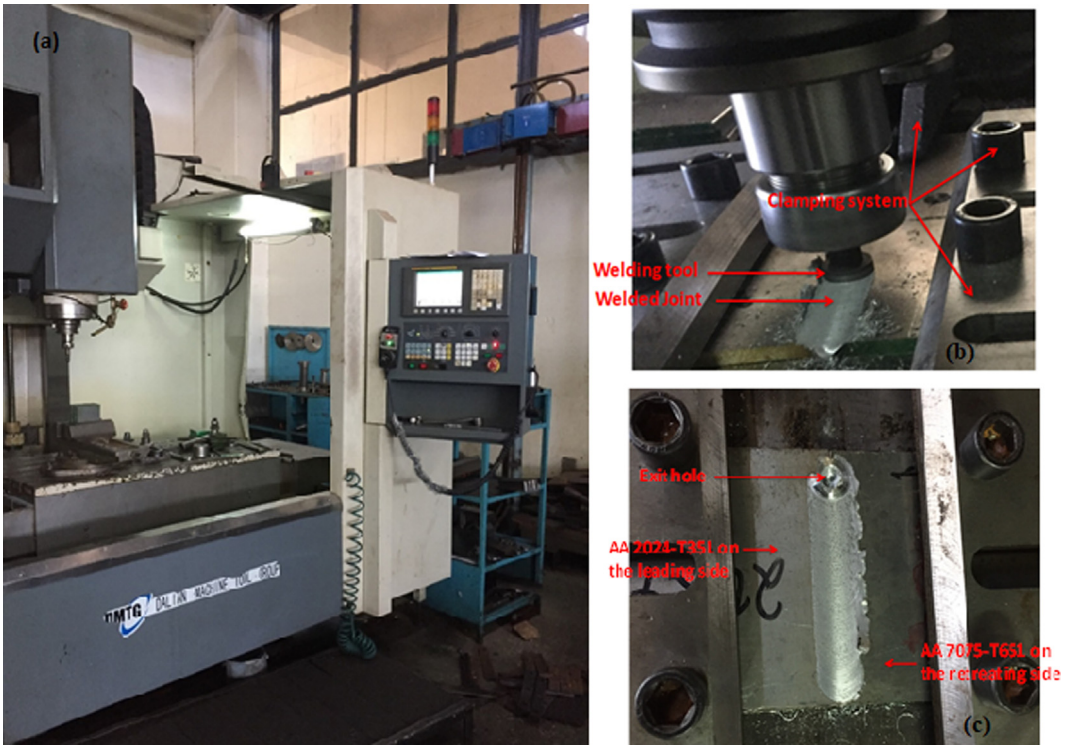

Fig. 3. (a) Fanuc oi-MC Control DMTG VDF- 1200 CNC Vertical Machining Center for FSW. (b) Friction stir welding process (c) FSWed joint.

2.5.2 Hardness test

The resistance of a substance to abrasion or penetration under localized pressure can be accurately, quickly, and affordably assessed using hardness tests. The most common method of determining a material's hardness is to gauge its resistance to being indented. Typically, the indenter is a ball, cone, or pyramid made of a material much harder than the one utilized. The test was done on the benchtop digital superficial Rockwell hardness tester of model HRMS-45 with ASTM E18 standards.

2.6 Surface topography in microscopic analysis

The surface morphology of the FSWed joint, Huvitz HRM-300 BF RL/TL model metallurgical microscope, and Zeta 20 3D optical profiler have been used. Figure 5 shows topographical data from the fractured surface of the welded

Table 3. Factors and levels of FSW.

Factors	Unit	Symbol	Level		
			Low	Medium	High
Rotational speed	(rpm)	A	800	1000	1200
Welding speed	(mm/min)	B	20	40	60
Plunge depth	(mm)	C	0.2	0.3	0.4

Table 4. Experimental results for FSW.

Run order	Input Parameters			Responses	
	A: Rotational speed (rpm)	B:Welding speed (mm/min)	C:Plunge depth (mm)	Ultimate tensile strength (UTS) (MPa)	Yield strength YS (MPa)
1	800	60	0.2	98.33	95.33
2	1200	60	0.2	78.65	74.00
3	1000	40	0.3	114.66	108.66
4	1000	40	0.3	119.33	109.66
5	1000	40	0.46	140.66	123.66
6	1000	40	0.3	112.66	102.56
7	1200	60	0.4	147.00	129.99
8	800	60	0.4	62.87	58.00
9	800	20	0.2	85.92	69.00
10	1000	40	0.3	114.66	104.33
11	800	20	0.4	56.23	51.25
12	1200	20	0.2	72.33	62.33
13	663.64	40	0.3	63.33	62.66
14	1000	73.64	0.3	71.18	67.74
15	1200	20	0.4	132.98	105.26
16	1000	6.364	0.3	55.95	47.67
17	1000	40	0.13	118.66	110.59
18	1336.36	40	0.3	119.83	104.00
19	1000	40	0.3	117.33	109.66
20	1000	40	0.3	114.66	113.67

joint. The sophisticated optical microscopes of this profiler's advanced camera produce high-quality images with no contact with the surface of the specimens. Then, interferometry techniques convert the captured images to vital information, such as height and surface roughness. The picture resolution at which the instruments capture the sample image is 1920×1440 pixels to observe the specimen at a suitable spatial resolution below $0.5\,\mu$m. A scanning electron microscope (JEOL JSM, IT 200, Japan) is used to evaluate the fractured surface of Al alloy weld joints.

3 Results and discussion

3.1 Model equations for FSW

A regression equation is a statistical technique for modeling the function of any physical phenomenon. This technique relates one or more independent variables to a dependent variable to formulate the system equation to predict a response. The following final model equations (Eqs. (2) and (3)) were developed to predict the UTS and YS of AA 2024-T351and AA 7075-T651 DFSW joints:

$$Y_{UTS} = +115.61 + 16.30 \times A + 4.76 \times B + 7.38 \times C + 24.27 \times A \times C - 8.87 \times A^2 - 18.78 \times B^2 + 4.59 \times C^2 \quad (2)$$

$$Y_{YS} = +110.13 + 12.27 \times A + 7.56 \times B + 4.82 \times C + 19.25 \times A \times C - 9.84 \times A^2 - 18.91 \times B^2. \quad (3)$$

The analysis of variance (ANOVA) is used to evaluate the model adequacy developed model to present the findings of the second-order response surface model fitting. Figure 6a–c displays the plots of the normal probability vs.

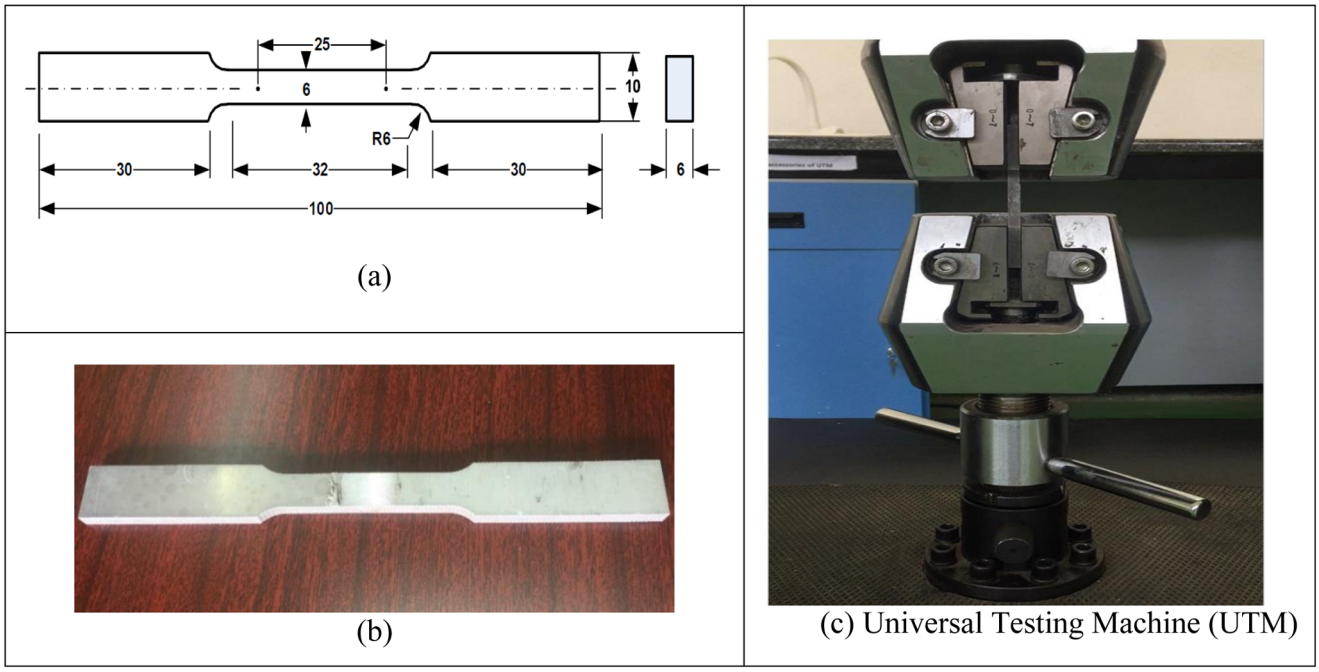

Fig. 4. (a) Schematic diagram of the ASTM E8/ E8M standard tensile test specimen. (b) Photograph of FSWed tensile specimen. (c) UTM.

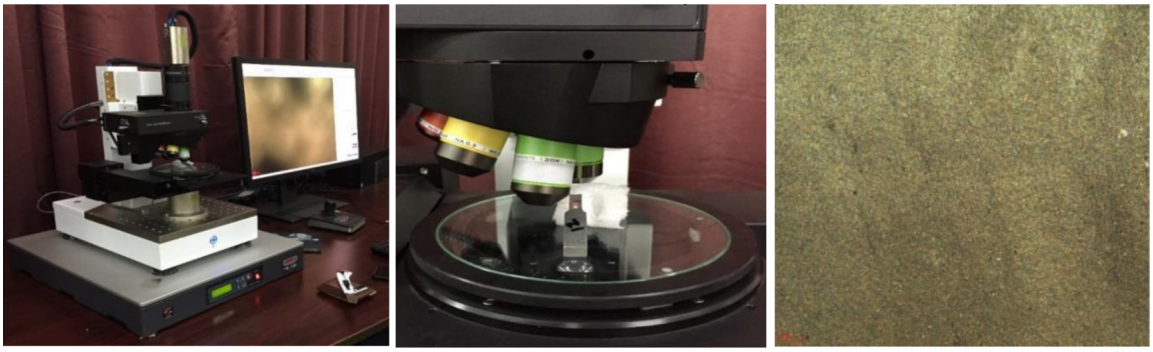

Fig. 5. (a) Zeta 20 3D optical profiler (b) Optical microscopic advanced camera probing the fracture surface of the specimen #12 with 50X magnification. (c) Fracture surfaces.

residuals; residual vs. predicted; and residuals vs. run value for UTS. The normality plot reveals that the residuals are close to the straight line, representing the model fit with data. The residuals are spread out, which suggests that they are independent, as shown in Figure 6b. The absence of unusual structures in Figure 6c indicates that the model is adequately presented.

3.2 The effect of FSW factors on UTS

The ANOVA was employed to test whether the different levels of treatment have any significantly different effect on the response variables. According to the ANOVA, Table 5, the *P*-value is less than 0.05; it indicates that the model is statistically significant. Hence, this suggests a significant difference between the levels of response variables. The experimental values provide an extremely accurate fit to the second-order response surfaces. The main factors and interaction of AC and higher orders of A^2, B^2, and C^2 significantly affect tensile strength. The remaining terms, which are insignificant, are eliminated through backward elimination processes. Figure 7 shows the interaction between RS and PD through the response surface and contour plot graphs. At lower RS, the tensile strength decreases while PD increases. Higher levels of PD and RS resulted in higher tensile strength. The main influences on tensile strength are rotational speed, welding speed [29–31], and plunge depth, which also significantly affect the TS of FSW processes [32].

The effect of tool rotational speeds, welding speeds, and tool plunge depth are investigated at three levels. The test results reveal a significant correlation: as tool rotation increases, tensile strength gets increases. The highest tensile strength value of 147 MPa was achieved at the

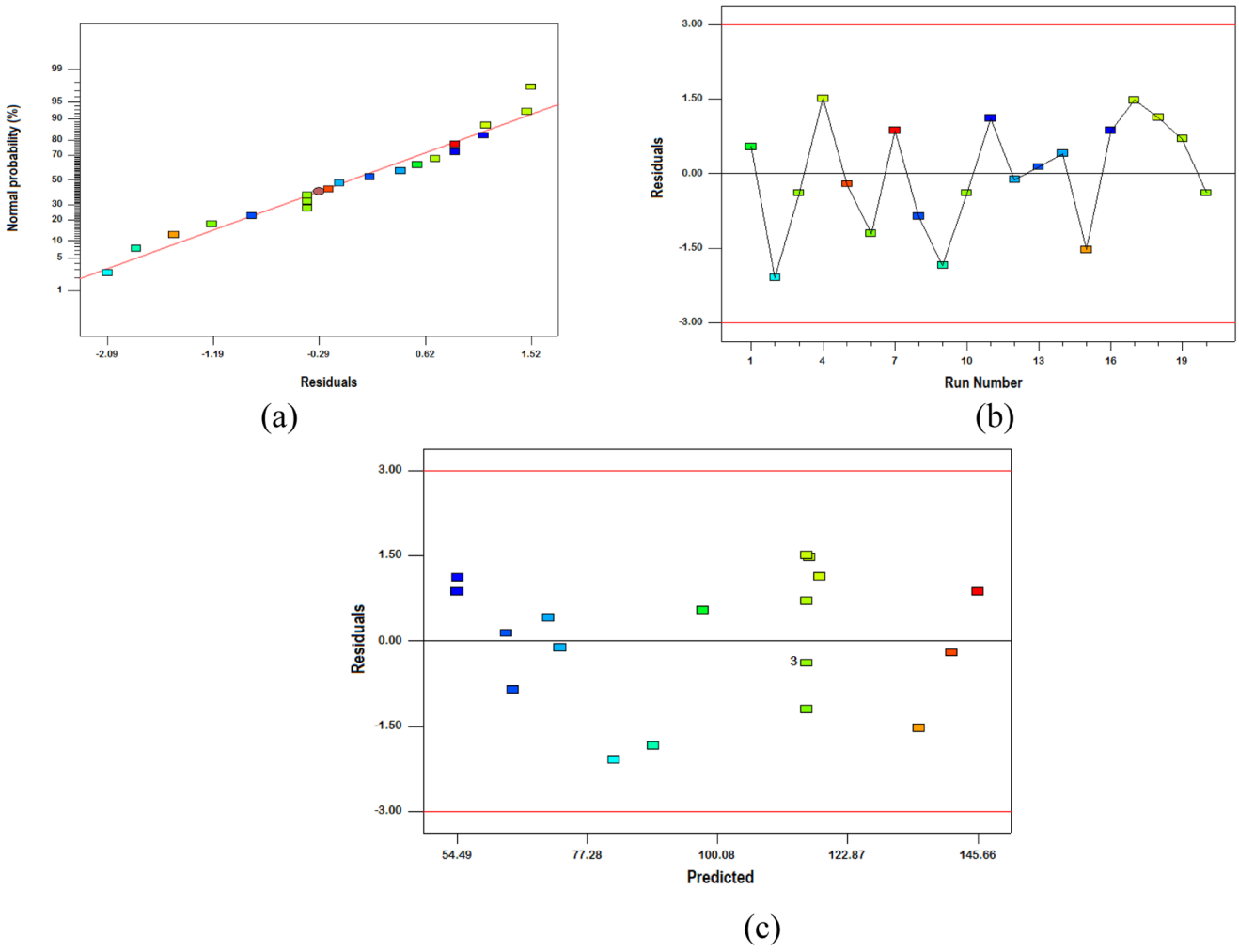

Fig. 6. (a–c) Residual graphs.

Table 5. ANOVA for UTS.

Source	SS	DOF	MS	*F*-Value	*P*-Value	Remark
Model	15929.45	7	2275.63	375.20	<0.0001	Significant
A:Rotational speed	3628.98	1	3628.98	598.34	<0.0001	
B:Welding speed	309.49	1	309.49	51.02	<0.0001	
C:Plunge Depth	744.80	1	744.80	122.80	<0.0001	
AC	4711.56	1	4711.56	776.83	<0.0001	
A^2	1135.10	1	1135.10	187.15	<0.0001	
B^2	5082.34	1	5082.34	837.97	<0.0001	
C^2	303.46	1	303.46	50.03	<0.0001	
Residual	72.78	12	6.06			
Lack of Fit	44.59	7	6.37	1.13	0.4624	
Pure Error	28.18	5	5.63			
Cor Total	16002.23	19				

DOF: degree of freedom; SS: sum of squares; MS: mean square.

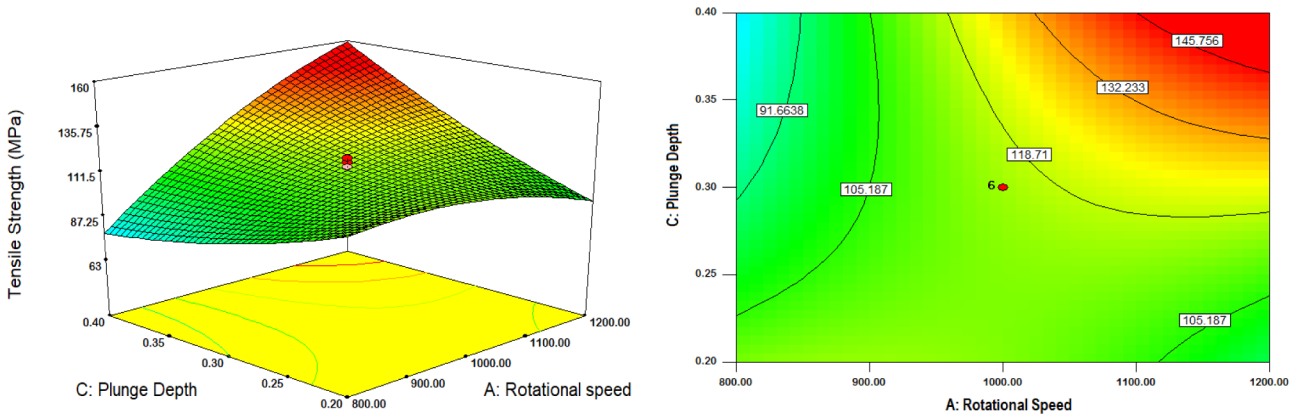

Fig. 7. Response surface and contour plot based on rotational speed and plunge depth for tensile strength.

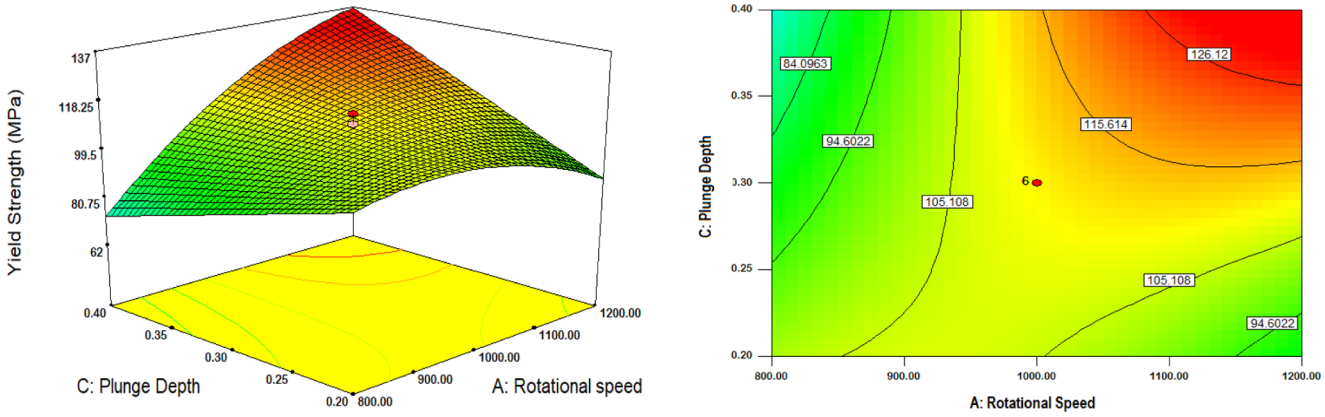

Fig. 8. Response surface and contour plot for yield strength (YS) based on RS and PD.

specific combination of welding parameters (1200 rpm, 60 mm/min, and 0.4 mm). This finding emphasizes the crucial role of welding parameters in determining joint strength. The FSW process, characterized by prolonged dynamic recrystallization and severe plastic deformation, leads to remarkable grain refinement. The degree of plastic deformation, influenced by the RS, affects material mixing and the amount of heat produced, which in turn softens the materials in the immediate surrounding area. Hamed [33] demonstrated that improved material mixing occurs in dissimilar FSWs with increased heat input. Similarly, there is a proportionate association between material mixing and tool RS [34,35]. Rodriguez et al. [35] observed that in FSWed different AA6061-AA7050 joints, increasing tool RS-enhanced material intermixing improves joint strength. Similar evidence was found on the maximum UTS of 92.9 MPa in DFSW of AA 6082-AA8011 at 1100 rpm, 60 mm/min [33]. The maximum UTS are 142 MPa with 5% elongation at 948 rpm and 85 mm/min using AA2024 and Copper materials [36]. Using optimum conditions of FSW of AA3003-AA6061, such as 1172 rpm, 57.44 mm/min TTA of 1.25° provides higher UTS of 95.8 MPa and 12.18% of elongation [31]. The FSW of AA 1050 at RS 1200 rpm and WS of 20 mm/min leads to 99.0 MPa UTS [37]. In addition, 124.9.0 MPa UTS was obtained with RS 900 rpm and WS 30 mm/min using AA100-AISI 304 [38]. The tensile strength values are 114–119 MPa at the medium level of FSW conditions. The FSW variables can be controlled by variations in the tool penetration depth, welding speed, and tool rotations, which can affect the joint's tensile strength [39]. The microvoids, dimples and cleavages were found at medium welding conditions (Fig. 12b). The lower tensile strength value (55.95 MPa) was obtained with the different combinations of rotational speed (1000 rpm), WS of 6.36 mm/min, and PD of 0.3 mm. This is mainly due to low welding speeds, which result in increased heat input and lead to flaws such as tunneling. Hence, the UTS values of DFSW are lower [40–43]. Too low welding speed (6.346 mm/min) deteriorates weld strength due to more heat input and slower cooling rates, causing excessive grain growth and reducing tensile strength of 55.95 MPa. More microvoids (Fig. 12a) are formed by improper stirring due to poor plastic flow of metal at higher welding speed, leading to lower welding strength.

3.3 The effect of FSW factors on YS

The lowest value of yield strength was due to the combining 1000 rpm rotational speed, 6.36 mm/min welding speed, and 0.3 mm plunge depth. The plunge depth was less of a significant and influential parameter on the yield strength

Table 6. ANOVA for YS.

Source	SS	DOF	MS	*F*-Value	*P*-Value	Remark
Model	12291.21	6	2048.536436	69.10	<0.0001	Significant
A:Rotational speed	2055.11	1	2055.119012	69.32	<0.0001	
B:Welding speed	780.47	1	780.4795711	26.32	0.0002	
C:Plunge Depth	317.30	1	317.3035877	10.70	0.0061	
AC	2964.69	1	2964.698726	100.00	<0.0001	
A^2	1410.63	1	1410.634415	47.58	<0.0001	
B^2	5201.97	1	5201.978589	175.47	<0.0001	
Residual	385.38	13	29.64477562			
Lack of Fit	304.27	8	38.03406038	2.34	0.1815	
Pure Error	81.10	5	16.22192			
Cor Total	12676.60	19				

of the FSWed joint. The relationship among the input parameters is shown in Figure 8 through the response surface and contour plot graphs. According to the ANOVA, Table 6, both the RS and WS are more influential on the response variables than the tool plunge depth for their P-values smaller than 0.05. The interaction between the RS, WS, and PD are plotted in the surface and contour graph shown in Figure 8. From the ANOVA Table 6, the main factors are RS, WS, and PD; the interaction of RS and PD; and higher orders of A^2 and B^2, which significantly affect yield strength. When the rotational speed increases, the YS tends to increase while increasing PD; there is less variation in YS. Similarly, increasing welding speed has a significant influence on YS. Higher YS were obtained at higher levels of RS and PD.

The combined effect of tool speed and traversal speed significantly affects the yield strength [44]. Consequently, yield strength could also increase if the welding and rotational speeds rise. When the tools rotational speed increases, frictional heat increases [39]. A deeper plunge results in enhanced material mixture in the joint seam due to frictional heating, producing higher yield strength. High levels of FSW conditions, such as 1,200 rpm, 60 mm/min, and 0.4 mm, produce the highest yield strength. The lowest yield strength was discovered at 1000 rpm, 6.36mm/min, and 0.3 mm, respectively, with a value of 47.67 MPa.

3.4 The influence of FSW factors on micro-hardness

Figure 9 shows the micro-hardness profile in the FSWed joint of AA2024-T351 and AA7075-T651. As depicted in Figure 9, the measurements were made, measuring the same distance on both sides of the weld centerline and comparing the results with the base material. In the TMAZ region of the FSWed joint of dissimilar aluminium alloy where coarsened precipitates are apparent, the micro-hardness value is comparatively greater than the stirred zone. This difference may precipitate hardened the base materials [45]. According to the micro-hardness values (HRB), the Weld Nugget Zone (WNZ) is found to have a hardness of 74.1 HRB, 75.5 HRB, and 80 HRB when stirred with low, medium, and high levels of FSW conditions,

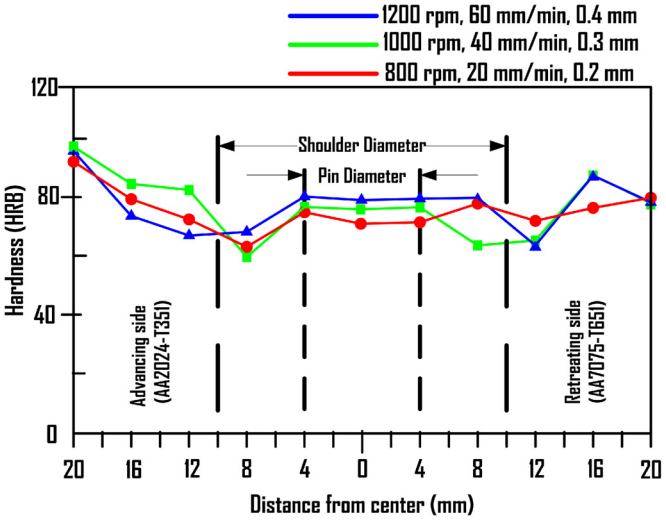

Fig. 9. The micro-hardness values of the FSWed joint.

respectively. The lowest rotational speed (800 rpm) was responsible for the lower hardness value record in the TMAZ section of the advancing side, where AA2024 was located. The 'W' shape pattern, Figure 9, is the most common profile phenomenon precipitation-hardened aluminium alloys experience during the FSW process [46]. The weld results show less microhardness (74.1–80 HRB) than the base material (95.7 HRB). This was explained by the fact that increased tool rotating speed causes a rise in localized heating, which causes grain growth and a reduction in microhardness in the WN zone [47,48].

Apart from grain refinement, the reduction in micro-hardness is produced by the over-aging effect caused by the frictional heat within the shoulder and tool interface. In contrast, high calefaction reduces microhardness by inducing strengthening precipitates to fragment and amalgamate [49,50]. The microhardness values are lower at low FS welding conditions than at middle and high FS welding conditions. This is because the smallest RS has

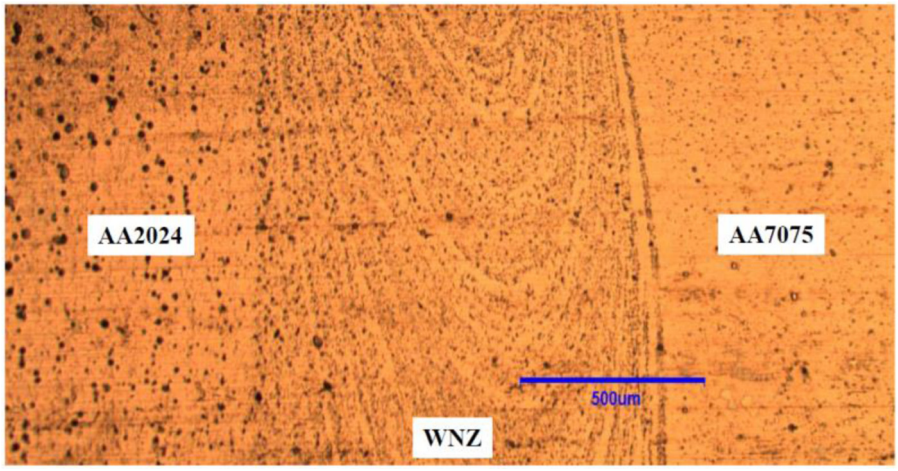

Fig. 10. Microscopic image of FSWed joint shows banded structure.

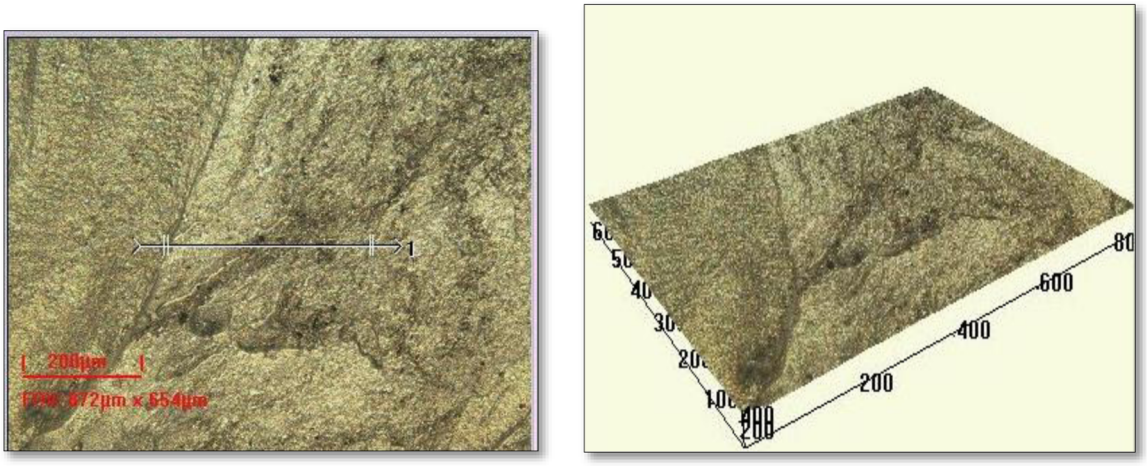

Fig. 11. The analysis report of Zeta 20 3D surface profiler.

minimal hardness values in DFSW. A similar observation was found at a welding speed of 60 mm/min; the optimum microhardness (132.5Hv) was predicted [51]. The optimal hardness values were 74.47 Hv, and the optimized values for TRS 1172 rpm, WS 57.44 mm/min, and tilt angle (TA) were 1.252° for FSW of AA 3003-6061 [28].

3.5 Surface topography

According to the image, the base metal of AA2024-T351 has a microstructure with coarse grain in the rolling direction than the base metal of AA7075-T651. Because of the considerable heat generation, alternating band structure with the microstructure of "onion rings," Figure 10, was seen in SZ at WS of 60 mm/min. Figure 11 is the Zeta 20 3D analysis report observed from the experimental investigation. This investigation found the lowest Ra value of 363.64 μm at the intermediate tool RS and WS, 1000 rpm and 40 mm/min. This average height is increasing further from the weld nugget zone. According to the surface profiler's image, flat sections consistent with the elongated grains are divided by ductile tear ridges that make up the fracture surface of the base material.

Figures 12(a–i) shows the microstructure of low (a–c), medium (d–f), and high (g–i) levels of parameters used during FSW. The Weld Nugget Zone is shown at the centre, free from defects in all values. The equiaxed grains with significantly smaller sizes predominate the area in contrast to huge and elongated grains of BM. The optical microstructural images to the left and right of the WNZ are the base material (BM) of AA2024-T351 and AA7075-T651. The parent material's optical picture, on the left and right side of a figure, showed an excellent distribution of tiny intragranular precipitates. The precipitate-free zone (PFZ) at the grain boundaries has expanded, and the strengthening precipitates have coarsened considerably in comparison to the microstructure of the parent material. On the micrograph image of the right side of the figure, elongated aluminium grains and a few fine Mg2Si precipitates were seen. A photo-micrograph of the WNZ and the interface junction of the AA7075-T651 alloy on the right side is displayed in Figures 12c, 12f, 12i. However, the grain was recrystallised on the opposite side because of the tool's rotating motion in the AA7075-T651 alloy. Compared to other welded joints made at different rotational speeds, the welded junction prepared at 1200 rpm rotational speed, 60 welding speed, and 0.4 mm tool plunge

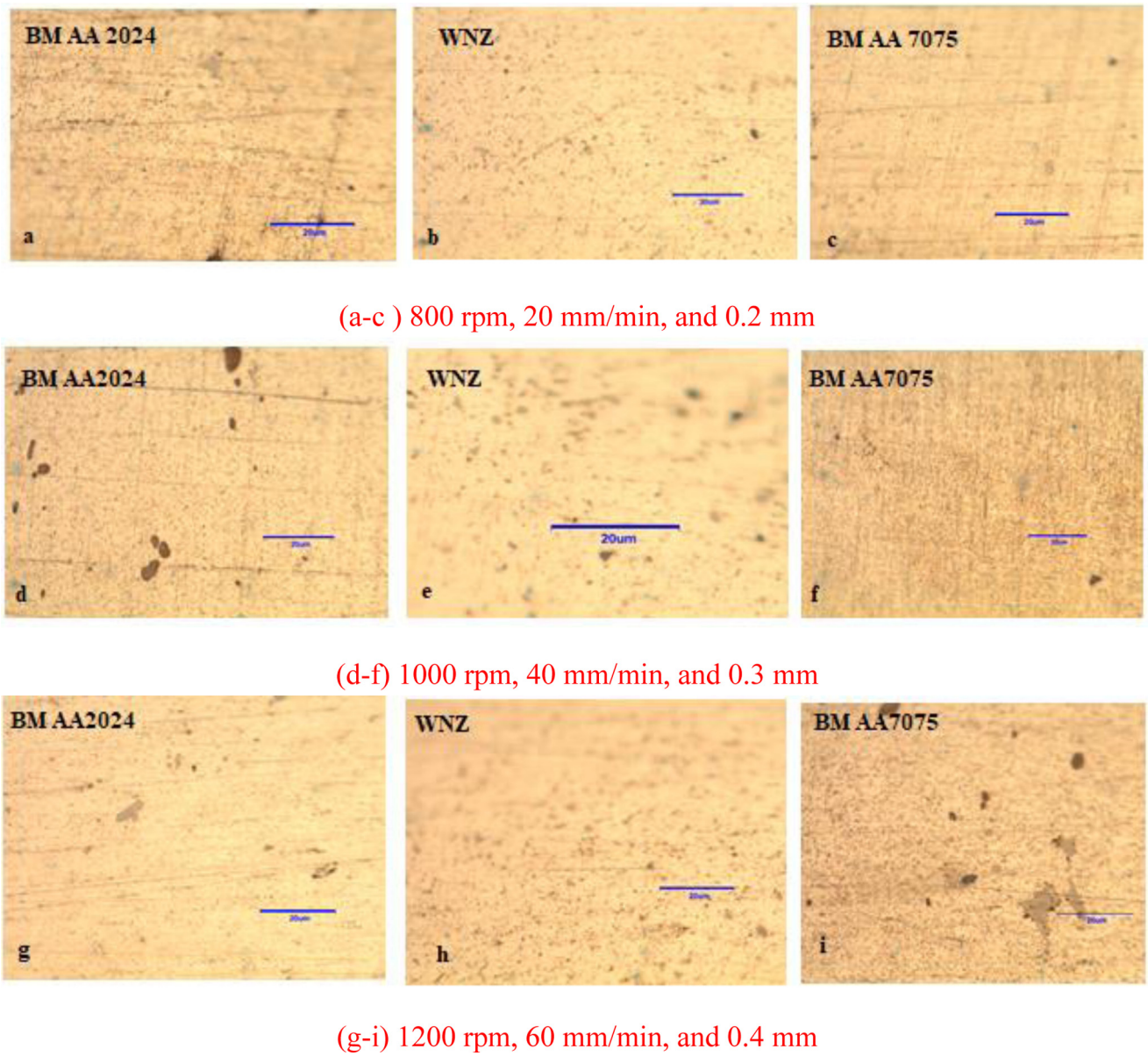

Fig. 12. (a–i) Optical Microstructures of different welding at different conditions.

depth had a smaller grain size, as shown in Figure 12h. This reduction in grain size indicates that the welded joints' tensile properties have improved [52].

Figures 13a–c shows the fractured surface morphologies of the FSWed dissimilar aluminum alloy joints using SEM at low, middle, and high welding conditions. The morphology of ductile failure was observed in all the specimens discussed, and it can be illustrated by the presence of dimples, cleavages, and microvoids [53,54]. More microvoids have been seen in Figure 13a at lower FS welding conditions. Figure 13a shows the numerous tiny dimples. This is consistent with the findings that the lower welding condition had the lowest elongation value and plastic deformation capability. The fracture surfaces at the middle welding conditions are shown in Figure 13b, and the tear ridge and dimples suggest that the fracture is ductile in contrast to the dimples seen in Figure 13a. The broader and deeper dimples in Figure 12c suggest that the material has more excellent toughness and flexibility at this depth.

The experimental results were validated using the optimal process variables for FSW using the desirability approach (Design Expert software). The optimum factors for maximum UTS and YS are RS 1192 rpm, WS 55.31 mm, and PD 0.4 mm.

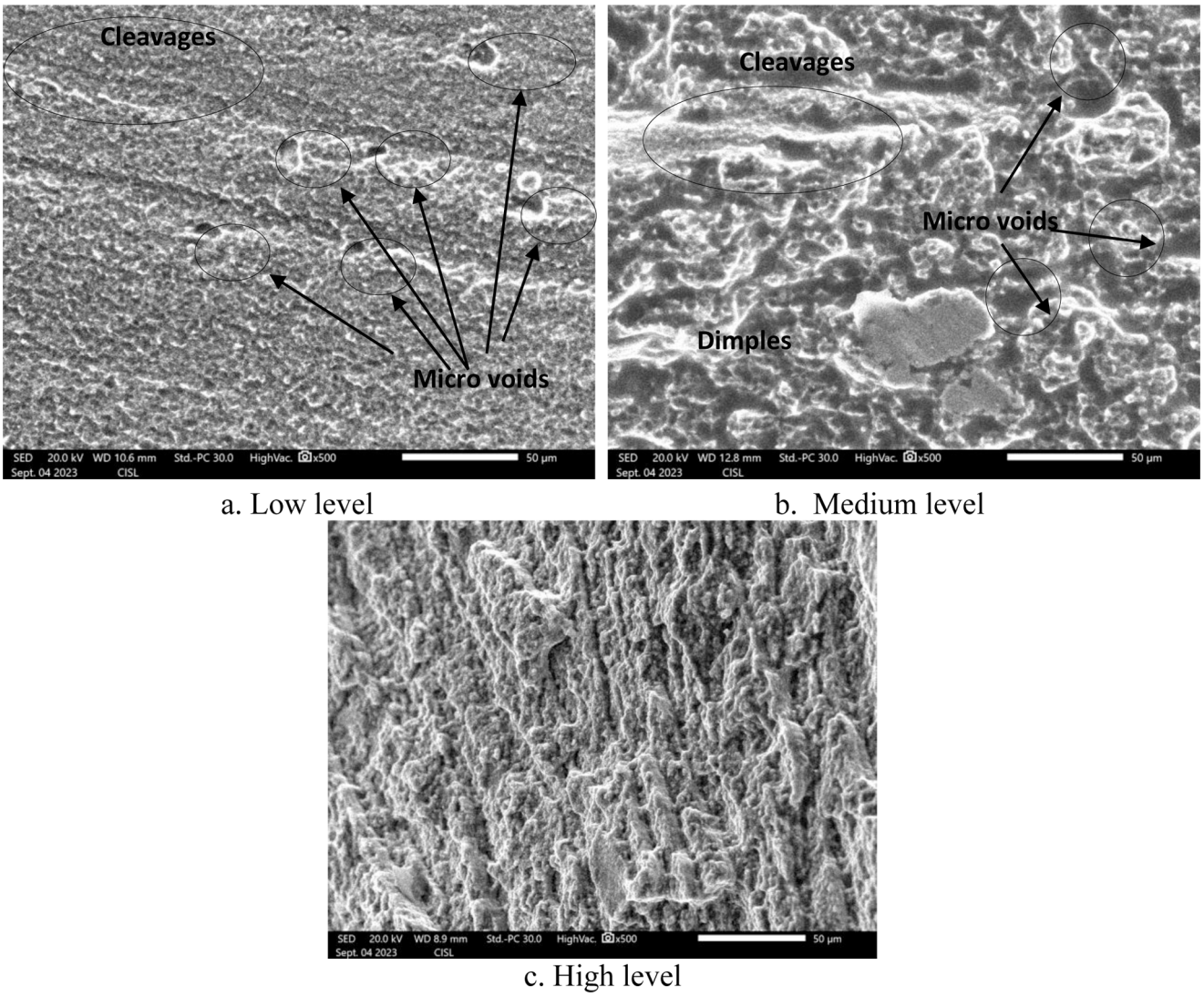

Fig. 13. (a–c) SEM images of fractured surfaces at different conditions.

4 Conclusion

This paper has investigated the effect of FSW factors on the mechanical properties of dissimilar aluminum alloys 2024-T351 and 7075-T651. The investigation's findings led to the following important conclusions.

- The mathematical, empirical relationships were constructed for the FSWed joint of AA2024-T351 and AA7075-T651.
- ANOVA analysis shows that the main factors interaction of RS and PD, quadratic terms of RS, WS, and PD, significantly affect UTS. In addition, the main factors, interaction of RS and PD, and quadratic terms of RS and WS have significant effects on YS.
- Maximum ultimate tensile strength of 147 MPa and yield strength of 129.99 MPa were found at RS 1200 rpm, WS 60 mm/min, and 0.4 mm tool plunge depth.
- The lower ultimate tensile strength of 55.95 MPa and yield strength 47.67 MPa was obtained at RS 1000 rpm, WS 6.364 mm/min, and PD 0.3 mm.
- The lowest welding speed (6.364 mm/min) caused the working temperature to increase for adequate softening and flow of materials.
- The lowest welding and rotational speeds were responsible for the resulting lower ultimate tensile strength.
- The hardness values of WZ are 74.1 HRB, 75.5 HRB, and 80 HRB for low, medium, and high FSW conditions, respectively.

Funding

The author(s) declare that no financial support was received for the research.

Conflicts of interest

The authors declare that they have no known competing financial interests or personal relationships that could have appeared to influence the work reported in this paper.

Data availability statement

Data will be made available on request.

Author contribution statement

Getachew Gebreamlak: Conceptualization, Investigation, Methodology, Validation, Writing–original draft. Sivaprakasam Palani: Conceptualization, Data curation, Formal Analysis, Investigation, Methodology, Supervision, Validation, Visualization, Writing–review and editing. Belete Sirahbizu: Supervision, Visualization, Writing–review and editing.

References

1. M.H. Abidi, N. Ali, H. Ibrahimi, S. Anjum, D. Bajaj, A.N. Siddiquee, A.U. Rehman, T-FSW of dissimilar aerospace grade aluminium alloys: influence of second pass on weld defects Metals, **10** (2020) 525
2. S.A. Manroo, N.Z. Khan, B. Ahmad, Study on surface modification and fabrication of surface composites of magnesium alloys by friction stir processing: a review, J. Eng. Appl. Sci. **69** (2022) 1–23
3. A.H. Karwande, S.S. Rao, Welding parameter optimization of alloy material by friction stir welding using Taguchi approach and design of experiments, AIP Conf. Proc. **1952** (2018) 020115
4. R.A. Gite, P.K. Loharkar, R. Shimpi, Friction stirs welding parameters and application: a review, Mater. Today: Proc. **19** (2019) 361–365
5. G. Cam, S. Mistikoglu, Recent developments in friction stir welding of Al-alloys, J. Mater. Eng. Perform. **23** (2014) 1936–1953
6. E.T. Akinlabi, R.M. Mahamood, Solid-state welding: friction and friction stir welding processes, Springer International Publishing, New York, NY, USA, 2020
7. Heidarzadeh, S. Mironov, R. Kaibyshev, G. Çam, A. Simar, A. Gerlich, P.J. Withers, Friction stir welding/processing of metals and alloys: a comprehensive review on microstructural evolution, Prog. Mater. Sci. **117** (2021) 100752
8. S.K. Das, S. Gain, P. Sahoo, Friction stir welding, Welding Technol. (2021) 1–39
9. P. Bahemmat, M. Haghpanahi, M.K. Besharati Givi, K. Reshad Seighalani, Study on dissimilar friction stir butt welding of AA7075-O and AA2024-T4 considering the manufacturing limitation, Int. J. Adv. Manufactur. Technol. **59** (2012) 939–953
10. E.J. Mueller, D.L. Seger, Metal fume fever—a review, J. Emerg. Med. **2** (1985) 271–274
11. K.P. Mehta, Sustainability in welding and processing, Innov. Manufactur. Sustain. (2019) 125–145
12. N.A. Liyakat, D. Veeman, Improvement of mechanical and microstructural properties of AA 5052-H32 TIG weldment using friction stir processing approach, J. Mater. Res. Technol. **19** (2022) 332–344
13. M.A. Wahid, N. Sharma, R. Shandley, Friction stir welding process effects on human health and mechanical properties, Int. J. Forensic Eng. Manag. **1** (2020) 42–52
14. K.N. Uday, G. Rajamurugan, Influence of process parameters and its effects on friction stir welding of dissimilar aluminium alloy and its composites − a review, J. Adhes. Sci. Technol. **37** (2023) 767–800
15. R. Anand, V.G. Sridhar, Studies on process parameters and tool geometry selecting aspects of friction stir welding − a review, Mater. Today: Proc. **27** (2020) 576–583
16. M.S. Mahany, R.R. Abbas, M.M.Z. Ahmed, H. Abdelkader, Influence of tool rotational speed and axial load in friction stir welding (FSW) of high strength aluminum alloys, Int. J. Res. Eng. Technol. **6** (2017) 114–120
17. A.M. Bayazid, M.M. Heddad, I. Cayiroglu, A review on friction stir welding, parameters, microstructure, mechanical properties, post weld heat treatment and defects, Mater. Sci. Eng. **2** (2018) 116–126
18. C. Zhang, G. Huang, Y. Cao, Y. Zhu, Q. Liu, On the microstructure and mechanical properties of similar and dissimilar AA7075 and AA2024 friction stir welding joints: effect of rotational speed, J. Manufactur. Process. **37** (2019) 470–487
19. M.M. Hasan, M. Ishak, M.R.M. Rejab, Effect of pin tool design on the material flow of dissimilar AA7075-AA6061 friction stir welds, IOP Conf. Ser.: Mater. Sci. Eng. **257** (2017) 012022
20. L. Cui, C. Zhang, Y.C. Liu, X.G. Liu, D.P. Wang, H.J. Li, Recent progress in friction stir welding tools used for steels, J. Iron Steel Res. Int. **25** (2018) 477–486
21. C. Zhang, G. Huang, Y. Cao, Y. Zhu, Q. Liu, On the microstructure and mechanical properties of similar and dissimilar AA7075 and AA2024 friction stir welding joints: effect of rotational speed, J. Manufactur. Process. **37** (2019) 470–487
22. G. Çam, G. İpekoglu, Recent developments in joining of aluminum alloys, Int. J. Adv. Manufactur. Technol. **91** (2017) 1851–1866
23. G. Cam, S. Mistikoglu, Recent developments in friction stir welding of Al-alloys, J. Mater. Eng. Perform. **23** (2014) 1936–1953
24. C. Zhang, G. Huang, Y. Cao, Q. Li, L. Niu, Q. Liu, Characterizations of microstructure, crystallographic texture and mechanical properties of dissimilar friction stir welding joints for AA2024 and AA7075 under different tool shoulder end profiles, Mater. Today Commun. **25** (2020) 101435
25. B. Anandan, M. Manikandan, Effect of welding speeds on the metallurgical and mechanical property characterization of friction stir welding between dissimilar aerospace grade 7050 T7651-2014A T6 aluminium alloys, Mater. Today Commun. **35** (2023) 106246
26. R.S. Kumar, T. Rajasekaran, S. Sivasubramanian, D. Garg, D. Gouda, R. Tiwari, A. Singh, Characteristic study of friction stir welding of aluminium alloy AA7075 using H13 surface hardened tool steel with variable tool pin design, IOP Conf. Ser.: Mater. Sci. Eng. **912** (2020) 032033
27. M.E. Matarneh, The effect of austenitization treatment temperature on H-13 tool steel's mechanical properties, Int. J. Mech. Appl. **6** (2016) 77–82
28. D.C. Montgomery, Design and analysis of experiments, John Wiley & Sons, 2017

29. D. Zlatanovic Labus, S. Balos, J.P. Bergmann, S. Rasche, M. Pecanac, S. Goel, Influence of tool geometry and process parameters on the properties of friction stir spot welded multiple (AA 5754 H111) aluminium sheets, Materials **14** (2021) 1157
30. M. Mohammadi Sefat, H. Ghazanfari, C. Blais, Friction stir welding of 5052-H18 aluminum alloy: modeling and process parameter optimization, J. Mater. Eng. Perform. **30** (2021) 1838–1850
31. A.N. Salah, H. Mehdi, A. Mehmood, A.W. Hashmi, C. Malla, R. Kumar, Optimization of process parameters of friction stir welded joints of dissimilar aluminum alloys AA3003 and AA6061 by RSM, Mater. Today: Proc. **56** (2022) 1675–1683
32. C. Guo, Y. Shen, W. Hou, Y. Yan, G. Huang, W. Liu, Effect of groove depth and plunge depth on microstructure and mechanical properties of friction stir butt weldedAA6061-T6, J. Adhes. Sci. Technol. **32** (2018) 2709–2726
33. J.A. Hamed, Effect of welding heat input and post-weld aging time on microstructure and mechanical properties in dissimilar friction stir welded AA7075-AA5086, Trans. Nonferrous Metal Soc. China **27** (2017) 1707–1715
34. Kalemba-Rec, M. Kopyscianski, D. Miara et al., Effect of process parameters on mech- anical properties of friction stir welded dissimilar 7075-T651 and 5083-H111 aluminum alloys, Int. J. Adv. Manuf. Technol. **97** (2018) 2767–2779
35. R.I. Rodriguez, J.B. Jordon, P.G. Allison et al., Microstructure and mechanical properties of dissimilar friction stir welding of 6061-to-7050 aluminum alloys, Mater. Des. **83** (2015) 60–65
36. R. Khajeh, H.R. Jafarian, S.H. Seyedein, R. Jabraeili, A.R. Eivani, N. Park, A. Heidarzadeh, Microstructure, mechanical and electrical properties of dissimilar friction stir welded 2024 aluminum alloy and copper joints, J. Mater. Res. Technol. **14** (2021) 1945–1957
37. X.C. Liu, Y.Q. Zhen, Y.F. Sun, Z.K. Shen, H.Y. Chen, G.U.O. Wei, W.Y. Li, Local inhomogeneity of mechanical properties in stir zone of friction stir welded AA1050 aluminum alloy, Trans. Nonferrous Metals Soc. China **30** (2020) 2369–2380
38. Datta, A. Shrivastava, N. Mandal, H. Roy, S.S. Chakraborty, A comparative investigation of butt friction stir welding of aluminium alloys, AA 1100 and AA 7075, with AISI 304 stainless steel, Weld. World **67** (2023) 1449–1465
39. M. Vahdati, M. Moradi, M. Shamsborhan, Modeling and optimization of the yield strength and tensile strength of Al7075 butt joint produced by FSW and SFSW using RSM and desirability function method, Trans. Indian Inst. Metals **73** (2020) 2587–2600
40. Forcellese, M. Simoncini, G. Casalino, Influence of process parameters on the vertical forces generated during friction stir welding of AA6082-T6 and on the mechanical properties of the joints, Metals **7** (2017) 350
41. M. Ghosh, M.M. Husain, K. Kumar et al., Friction stir-welded dissimilar aluminum alloys: microstructure, mechanical properties, and physical state, J. Mater. Eng. Perform. **22** (2013) 3890–3901
42. M. Saeidi, B. Manafi, M.B. Givi et al., Mathematical modeling and optimization of friction stir welding process parameters in AA5083 and AA7075 aluminum alloy joints, Proc. Inst. Mech. Eng. B **230** (2016) 1284–1294
43. Z. Zhu, H. Zhang, T. Yu et al., A finite element model to simulate defect formation during friction stir welding, Metals **7** (2017) 256
44. Bhojan, N. Senthilkumar, B. Deepanraj, Parametric influence of friction stir welding on cast Al6061/20% SiC/2% MoS2 MMC mechanical properties, Appl. Mech. Mater. **852** (2016) 297–303
45. P. Avinash, M. Manikandan, N. Arivazhagan, K.D. Ramkumar, S. Narayanan, Friction stir welded butt joints of AA2024 T3 and AA7075 T6 aluminum alloys, Proc. Eng. **75** (2014) 98–102
46. P.S. De, R.S. Mishra, Friction stir welding of precipitation strengthened aluminium alloys: scope and challenges, Sci. Technol. Welding Joining **16** (2011) 343–347
47. T. Singh, S.K. Tiwari, D.K. Shukla, Preparation of aluminum alloy-based nanocomposites via friction stir welding, Mater. Today Proc. **27** (2020) 2562–2568
48. Sharma, V.M. Sharma, S. Mewar et al., Friction stir processing of Al6061- SiC −graphite hybrid surface composites, Mater. Manuf. Process. **33** (2018) 795–804
49. D.F. Scialpi, P. Cuomo, P.D. Summa, Micro-friction stir welding of 2024–6082 aluminum alloys, Weld Int. **21** (2008) 16–22
50. T. Singh, S.K. Tiwari, D.K. Shukla, Novel method of nanoparticle addition for friction stir welding of aluminium alloy, Adv. Mater. Process. Technolog. **8** (2022) 1160–1172
51. V. Haribalaji, S. Boopathi, M.M. Asif, Optimization of friction stir welding process to join dissimilar AA2014 and AA7075 aluminum alloys, Mater. Today: Proc. **50** (2022) 2227–2234
52. M. Ryan, S. Suresh, K. Kumar, Microstructural investigations on friction stir welded aluminium alloy, J. Ind. Pollution Control **33** (2017) 1772–1774
53. Y. Yan, H. Li, J. Zhang, N. Kong, The effect of initial annealing microstructures on the forming characteristics of Ti-4Al-2V, Titanium Alloy Mater. **576** (2019) 1–12
54. H.J. Zhao, B.Y. Wang, G. Liu, L. Yang, W.C. Xiao, Effect of vacuum annealing on microstructure and mechanical properties ofTA15 titanium alloy sheets, Trans. Nonferr. Metal Soc. China **25** (2015) 1881–1888

Cite this article as: Getachew Gebreamlak, Sivaprakasam Palani, Belete Sirahbizu, Mechanical characteristics of dissimilar friction stir welding processes of aluminium alloy [AA 2024-T351 and AA 7075-T651], Manufacturing Rev. **11**, 19 (2024)